FEATURE ARTICLE

Multi-Scale Model for Binary Mixtures Containing Nanoscopic Particles

Anna C. Balazs,*,† Valeriy V. Ginzburg,† Feng Qiu,† Gongwen Peng,† and David Jasnow‡

Department of Chemical and Petroleum Engineering, University of Pittsburgh, Pittsburgh, Pennsylvania 15261, and Department of Physics and Astronomy, University of Pittsburgh, Pittsburgh, Pennsylvania 15260

Received: September 20, 1999; In Final Form: December 9, 1999

We develop a computer simulation for the dynamic behavior of a phase-separating binary mixture that contains mobile, solid particles. The system models "filled polymers", which contain not only a blend of different macromolecules, but also solid fillers. We focus on the case where one of the components preferentially wets the surface of the particles. By combining a mesoscopic, coarse-grained description of the fluids with a discrete model for the particles, we show that the addition of hard particles significantly changes both the speed and the morphology of the phase separation. To probe the late-stage properties of the system, we also develop a mean-field rate-equation model for the mixture. The results indicate that the phase separation is arrested in the late stage; the "steady-state" domain size depends strongly on both the particle diffusion constant and the particle concentration. To obtain insight into the effects of processing on the properties of such composites, we also investigated the behavior of the binary fluid/particle mixture under shear. For sufficiently large particle densities, we find that the anisotropic growth caused by the imposed shear is destroyed by the randomly moving particles, and the domains are isotropic in shape even for large shear strains. Finally, we apply our models to mixtures of diblock copolymers and fillers. Overall, our findings reveal how the solid additives can be used to tailor the morphology of the complex mixture, and thereby control the macroscopic properties (such as mechanical integrity) of the composite.

Introduction

The fabrication of typical polymeric products requires the intermixing of several macromolecular fluids, as well as the addition of solid "filler" particles.[1] By blending different polymers, the properties of the material can be tailored by varying the relative amount and type of macromolecules in the mixture.[2] Furthermore, the performance of a high-cost polymer can be extended by combining it with a low-cost component. By adding solid fillers, the mechanical, thermal, and interfacial properties of the material can be dramatically improved relative to the pure polymer blend.[1] For example, in the case of polymer/clay composites, the addition of just 2−5 wt % of nanoscopic clay fillers doubles the tensile strength and modulus,[3] triples the heat distortion temperature,[3] and reduces the gas permeability by a factor of 2.[4] As other examples, nanoscopic rubber particles are commonly added to enhance toughness, and carbon black is used to improve the processibility of blends.[5] Despite the advantages offered by such "filled" systems, surprisingly little is known about the factors that control the morphology, the phase behavior, and ultimately, the properties of the material. As a consequence, the development of filled polymers and composites for specific applications remains an empirically driven process that is both costly and inefficient.

The lack of information on these systems is due to the complexity of the interactions that occur within the molten mixtures. Most polymer pairs are immiscible, and thus, the filled systems include phase-separating fluids that are far from equilibrium. The nanoscale solid fillers are mobile and can interact among themselves and with the fluids. Thus, to understand the behavior of filled systems, it becomes necessary to focus on the *dynamic* properties of solid particles in a *phase-separating* fluid mixture.

While phase separation in binary fluids has been studied extensively through theoretical and experimental methods,[6] there have been few systematic investigations into the influence of solid additives on the mixtures. Recent studies have shed light on the interactions between a phase-separating fluid and a stationary wall,[7a] substrate,[7b,c] or sphere,[7d,e] but much less is known about the kinetics of mixtures that contain *mobile particles* that are *tens of nanometers to microns* in size. To address this problem, Tanaka et al.[8] examined the properties of a polymeric mixture undergoing a critical quench in the presence of glass beads, which are preferentially wet by one of the components. Their results revealed that even a small concentration of hard particles significantly changes the morphology and dynamics of the phase separation process. Recently, Karim et al.[9a] probed the properties of *immobile* fillers in an immiscible polymer blend and found that nanoscopic fillers induce the formation of novel patterns within the mixture. New experiments are currently under way to explore the rich behavior to be found in polymer blends containing *mobile* fillers.[9b]

To model and investigate the behavior of this complex system, we recently developed a computer simulation for the dynamic

* Corresponding author.
† Department of Chemical and Petroleum Engineering.
‡ Department of Physics and Astronomy.

10.1021/jp993356+ CCC: $19.00
Published on Web 02/01/2000

behavior of a binary, phase-separating mixture containing hard, mobile particles.[10] Unlike earlier dynamical models of ternary systems (describing, e.g., oil−water−surfactant mixtures),[11,12] we explicitly take into account the "excluded volume" interaction between the particles and the background fluid. The motion of these particles influences the behavior of the fluids, and the thermodynamic and kinetic properties of the fluids in turn affect the movement of the particles. The model allows us to incorporate and vary such features as (1) the wetting interactions between the particles and the fluids, (2) long-range forces (van der Waals or electrostatic) between the particles, (3) the size and shape of the particles, and (4) the composition of the mixture. We can also introduce simple shear and other externally applied flows. Using this model, we can isolate factors that control the growth of the fluid domains, the dispersion of the particles, and the structure of the solid−liquid and liquid−liquid interfaces. Thus, we can determine the important processes that govern the temporal evolution of the mixture. By considering the effect of shear and other imposed flows, we can also analyze how processing affects the morphology of the mixture and the formation of homogeneous composites.

To complement this computational approach, we also developed a mean-field kinetic rate-equation model to characterize the effect of the particles on the structure of the fluid mixture.[13] The analytical model provides additional insight into the late-stage behavior of the system.

Below, we begin by describing the different models we used to analyze the behavior of these complex mixtures. We then consider the properties of the systems in the absence and presence of imposed flow fields, such as shear. Finally, we apply our methods to mixtures of particles and diblock copolymers. The latter studies can facilitate the fabrication of novel composites that contain alternating, nanoscale domains of polymeric and metallic materials.

The Models

Simulations. Our multi-scale simulation couples a coarse-grained description of the fluids with a discrete model for the particles. A coarse-grained, mesoscopic description is particularly appropriate for the case of polymer blends, where the time scale for the deformation of the polymer domains is longer than the characteristic time for the motion of an individual chain, and the size of the domains is large compared to the size of the individual chains.[14] On the other hand, it is important to explicitly take into account the size and shape of the fillers, as well as pairwise interactions between these particles. Hence, for the solid additives, we turn to a Brownian dynamics model, which describes the motion of each individual particle under the influence of all the forces acting on the system. Below, we describe the different methods in more detail and discuss how the models are integrated so that the evolution of the fluid domains is affected by the particles and the motion of the particles in turn is coupled to the phase separation of the binary mixture.

Our description of the fluid is based on the Cahn−Hilliard approach;[15] we consider a phase separating, symmetric binary AB mixture characterized by the scalar order parameter $\psi(\mathbf{r})$. This parameter represents the difference between the local volume fraction of A and B at a position $\mathbf{r}$: $\psi(\mathbf{r}) = \phi_A(\mathbf{r}) - \phi_B(\mathbf{r})$. Note that $\psi = \pm \psi_{eq}$ corresponds to the equilibrium order parameter for the A-rich (B-rich) phase. (In studies described below, we chose $\psi_{eq} = 1$.) In the Cahn−Hilliard model, the phase separation dynamics are described by the following equation:

$$\partial\psi/\partial t = M \nabla^2 (\delta H\{\psi\}/\delta\psi) + \xi \quad (1)$$

where M is a kinetic coefficient (taken as a constant for simplicity), and ξ is a conserved zero mean Gaussian white noise. The free-energy functional $H\{\psi\}$can be written as the sum of two terms: $H\{\psi\} = H_{GL}\{\psi\} + H_{CPL}\{\psi\}$. The first term is the usual Ginzburg−Landau functional

$$H_{GL}\{\psi\} = \int [f(\psi) + c\,(\nabla\psi)^2/2]\, d^d\mathbf{r}, \quad \text{with } f(\psi) = -a\,\psi^2/2 + b\,\psi^4/4 \quad (2)$$

and d is the spatial dimensionality, which we take as $d = 2$ in the simulations reported here. The second term, $H_{CPL}\{\psi\}$, takes into account the coupling between the particles and the order parameter field and is given by

$$H_{CPL}\{\psi\} = \Sigma_i \int d^d\,\mathbf{r}\, V(\mathbf{r} - \mathbf{R}_i)\,(\psi(\mathbf{r}) - \psi_s)^2 \quad (3)$$

Here, $\mathbf{R}_i$ is the position of the center of mass of the ith particle and ψ_s is the order parameter at the surface of the particle. The summation is over all particles. For short-ranged interactions, we can take

$$V(\mathbf{r}) = \mathrm{C}\,\exp(-|\mathbf{r}|/r_0) \quad (4)$$

where C is a constant and r_0 represents a microscopic length scale. A variety of alternative choices for $V(\mathbf{r})$ will yield the same qualitative features.

In the present studies, the particles are spherical in shape and have a radius of R_0. To describe their interaction with the background fluid, we impose the following boundary conditions. First, the order parameter at the surface of each particle is set to a constant value, i.e, $\psi_s = 1$. In effect, the particles are "coated" by a layer of A and thus, are wet by the A fluid. We note that, in the available experiments,[8,9a] the particles are also wet by one of the components in the binary mixture. Thus, in this respect, we can compare our results to the experimental data. Second, we stipulate that there is no flux of the order parameter into the particles by setting $\partial_n\mu(\mathbf{r},t) = 0$ at the surface of each particle, where $\mu = (\delta H/\delta\psi)$ is the chemical potential and ∂_n denotes the surface normal derivative. Combined, the two boundary conditions ensure both the excluded volume requirement and conservation of the order parameter.

The particles exert an influence on the binary mixture through the above boundary conditions (wetting and excluded volume effects). In addition, through eqs 2−4, we see that the free energy of the system is reduced when the value of ψ near a particle is similar to the value of ψ_s. Thus, the nature and extent of the wetting interaction plays a role in the evolution of the fluid domains. We note that the value of ψ_s can be varied to model different interfacial behavior between the fluids and the particles. (For example, setting $\psi_s = 0$ favors the localization of the nanoscale particles at the interfaces between the two fluids.)

These particles undergo Brownian dynamics and their motion is described by the following Langevin equation (in the high friction limit, where the inertial term can be neglected):

$$\mathrm{d}\mathbf{R}_i/\mathrm{d}t = M_p\,(\mathbf{f}_i - \partial H_{CPL}/\partial\mathbf{R}_i) + \eta_i \quad (5)$$

where M_p is mobility, $\mathbf{f}_i$ is the force acting on the i th particle due to all the other particles, and η_i represents a Gaussian white noise. The second term is the force from the fluid that modifies the motion of the particles. In effect, $(-\partial H_{CPL}/\partial\mathbf{R}_i)$ represents

a thermodynamic force that drives the particles into the compatible, wetting phase.

The current simulation is carried out in two dimensions; our lattice is 256 × 256 sites in size, with periodic boundary conditions in both the x and y directions. A cell dynamical systems (CDS) method[16] is used in place of a direct forward integration of eq 1 to update the value of ψ for the phase-separating AB mixture. By employing CDS modeling (rather than a conventional discretization of eq 1), we can increase the computational speed of the simulation. To simulate the particle dynamics, we discretize eq 5 and only allow the particles to move between different lattice sites. A "Kawasaki exchange" mechanism is used for each particle move: first, the order parameter values from all the cells to be occupied by a particle in its "new" position are moved to the "old" particle position. Next, the boundary conditions are imposed at the "new" position. This mechanism ensures the conservation of the order parameter. Such dynamics may break down for large particle mobilities, so we considered only the case where the diffusion constant is rather low (almost all particle "jumps" are to neighboring sites).

The discretized equations of motion for the system have the following form,

$$\psi(\mathbf{r}, t+1) = F[\psi(\mathbf{r},t)] - \ll F[\psi(\mathbf{r},t)] - \psi(\mathbf{r},t) \gg + \xi(\mathbf{r},t)$$

$$\mathrm{F}[\psi(\mathbf{r},t)] = g(\psi(\mathbf{r},t)) - \delta H_{\mathrm{CPL}}/\delta\psi + c(\ll \psi(\mathbf{r},t) \gg - \psi(\mathbf{r},t))$$

$$\mathrm{g}(\psi) = \zeta \tanh(\psi)$$

$$\mathbf{R}_i(t+1) = \mathbf{R}_i(t) + \mathrm{M_p}\,(\mathbf{f}_i - \partial H_{\mathrm{CPL}}/\partial \mathbf{R}_i) + \eta_i(\mathbf{r},t) \quad (6)$$

where $\ll * \gg$ is the isotropic spatial average over the nearest neighbor and the next-nearest neighbor sites, and $[\ll * \gg - *]$ can be thought of as a discretized generalization of the Laplacian.

The function $F(\psi)$ in eq 6 plays the role of the chemical potential. It has a local driving term $g(\psi)$ and a term arising from the interaction with other sites; the map $g(\psi)$ controls the local order parameter dynamics of each site. The function $g(\psi)$ has a single unstable fixed point and two stable fixed points located on each side of the unstable fixed point. Its exact functional form is not important for studying the universal properties of the phase separation dynamics.[16] Here, we select the map $g(\psi) = \zeta \tanh(\psi)$, with $\zeta < 1$ above the critical temperature, and $\zeta > 1$ below.

During the processing of polymer/particle mixtures, the system is subjected to various flow fields. At the simplest level, one can incorporate the effects of flow by adding an advective term to the equation of motion. Introducing the advective term into eq 1 yields[14,17]

$$\partial\psi/\partial t + \mathbf{v}\cdot(\nabla\psi) = M\,\nabla^2\,(\delta H\{\psi\}/\delta\psi) + \xi(\mathbf{r},t) \quad (7)$$

To initiate our studies, we will consider an imposed shear flow that is characterized by the following fixed velocity field:[14,17,18]

$$v_x(\mathbf{r}) = S(t)y, \quad v_y = 0 \quad (8)$$

where the shear rate $S(t)$ is a given function of time. These equations can be discretized and then readily forward integrated in time by a variety of numerical techniques.[16,19]

In the presence of shear flow, eq 5 now becomes

$$(\mathrm{d}\mathbf{R}_i/\mathrm{d}t - \mathbf{v}(\mathbf{R}_i)) = M_{\mathrm{p}}\,(\mathbf{f}_i - \partial H_{\mathrm{CPL}}/\partial \mathbf{R}_i) + \eta_i(\mathbf{r},t) \quad (9)$$

where $\mathbf{v}(\mathbf{R}_i)$ (given by eq 8) is the systematic velocity that carries the particle along as the mixture is being sheared. (More generally, it is the local flow field.) Thus, in the presence of an imposed shear, eqs 7 and 9 constitute the coupled set of equations that are solved numerically to yield the dynamic behavior of the system.

In the studies described below, we consider separately cases in which $H_{\mathrm{CPL}} = 0$ and $H_{\mathrm{CPL}} \neq 0$ in eq 3. For the cases in which $H_{\mathrm{CPL}} = 0$, the motion of the particles is purely diffusive because we neglect the forces exerted by the fluids on the solids. In the case where $H_{\mathrm{CPL}} \neq 0$, the osmotic effects in the fluid couple back on the motion of the particles. [For $H_{\mathrm{CPL}} \neq 0$, the diffusivity of the particles can, however, be enhanced by increasing the magnitude of the noise (i.e., temperature) acting on the particle, as indicated in eq 5.] In physical terms, the value of H_{CPL} is a measure of the strength of the interaction between the coated particles and the A fluid; a larger value of H_{CPL} (or coupling constant C) indicates a stronger interaction between the fillers and the compatible fluid.

Kinetic Equations. For the case of $H_{\mathrm{CPL}} = 0$, we also developed a set of kinetic equations to describe the behavior of the 50:50 mixture.[13] Here, we assume that the particle concentration, n, is small, i.e., the interparticle distance $n^{-1/d} \gg R_0 > \lambda$, where λ is the width of an AB-interface. The A-coated particles move diffusively, with a diffusion constant D. The system separates into A-rich and B-rich domains. Let $N_-(t)$ be the total number of particles that are in B-rich (nonwetting) domains at time t. Likewise, let $N_+(t) = N - N_-(t)$ be the total number of particles that are in A-rich domains and note $n_+(t) = N_+(t)/L^d = n - n_-(t)$. Here, L is the system size, and d is the space dimensionality. In the following, we set $d = 2$, although the theory can be easily extended to any dimensionality.

The densities $n_+(t)$ and $n_-(t)$ change due to the motion of the particles and the interfaces. Such changes can be described as "reactions" of particles with interfacial segments. Since these "reactions" involve interfaces, they also affect the domain growth and coarsening rate. In particular, one can expect that when the number density of particles and their mobility increase, the coarsening rate would slow down at the very late stage of the phase separation; this conclusion is confirmed by our simulations.[10,13]

To derive mean-field kinetic equations for this system, we consider the two most elementary processes between particles and interfaces. In the first one (Figure 1a), particles simply jump over the nearest interface. If we denote the particle in the A-rich phase as A, the particle in the B-rich phase as B, and the interface segment as C, the reaction can be written as

$$A + C \leftrightarrow B + C \quad (10)$$

with reaction constants k_1 and k_{-1} for the respective direct and the inverse reactions. In the second reaction (Figure 1b), the boundary layer of a B particle merges with the A-domain, increasing the total length of the interface between the two domains. The reaction can be written as:

$$B + C \rightarrow A + lC \quad (11)$$

where k_2 is the reaction constant, and l is the number of the newly created interfacial segments. In the reverse reaction, new interfaces would be created by having a B "foot" extend into the A phase and engulf an A-coated particle. The latter reaction can be disregarded since the probability of the incompatible phase spontaneously "surrounding" an A particle is extremely small, especially at the late stage, where interfaces are relatively "flat". (In fact, taking the reverse reaction into account does

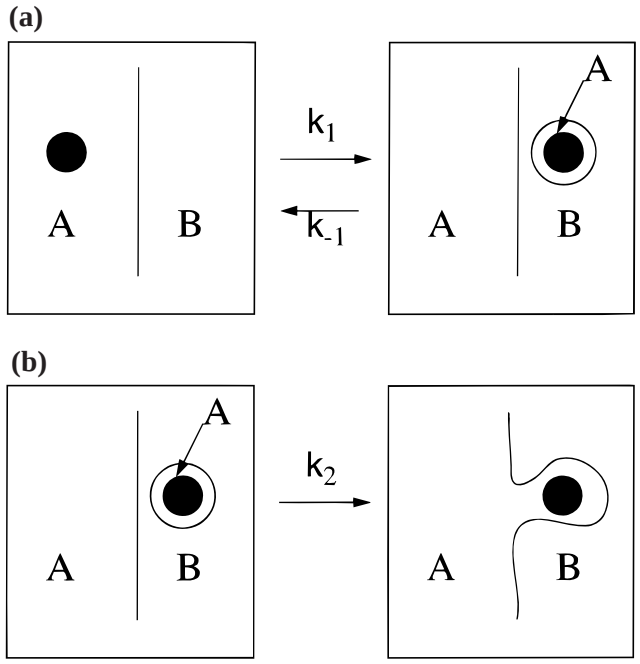

Figure 1. Elementary processes in the particle−interface interaction: (a) a particle "jumps" over the interface, and (b), the interface "overtakes" the B-particle. Note that the particles are wet by component A.

not change the qualitative results but merely renormalizes the effective domain growth rate.)

To write down kinetic equations, we introduce a new variable, the "interface area density" $\sigma = S/L^d$, where S is the total area of all AB interfaces, and L is the system size. This variable is inversely proportional to $R(t)$, the characteristic domain size, $\sigma \sim 1/R(t)$.[20] In the absence of particles, σ decreases according to the Lifshitz−Slyozov law:[21] $\sigma \sim t^{-1/3}$. When particles are present, additional interfaces are created according to reaction 11, and the overall evolution of σ can be approximated by the following differential equation:

$$d\sigma/dt = - A\,\sigma^4 + k_2\, n_-(l-1)\,\sigma \qquad (12)$$

The proportionality constant A has dimensionality L^3t^{-1} and describes the growth of the characteristic size in a particle-free system ($n_+ = n_- = 0$). The concentration of the particles in the B-phase is described by a second kinetic equation:

$$d\, n_-/dt = - k_2\, n_-\,\sigma - k_{-1}\, n_-\,\sigma + k_1\, n_+\,\sigma \qquad (13)$$

and $n_+ = n - n_-$. Equations 12 and 13 must be supplemented with initial conditions for $\sigma(t = 0)$ and $n_-(t = 0)$.

Although these equations are nonlinear, and the general analytical solution cannot be obtained, we can study the fixed points and analyze the evolution of the system numerically by integrating eqs 12 and 13. The resulting values for $R(t)$ and $n_-(t)$ are compared with the simulation data in the Results and Discussion section. To find the fixed points of the system of eqs 12 and 13, we set the right-hand sides of both equations to zero. It is possible to solve the two equations exactly, and thus find that there is one (linearly) stable "interior" fixed point. We discuss this result in the section below.

Results and Discussion

Spherical Particles in a Binary Mixture. Through the simulations, we consider the influence of particles on the evolution of a 50:50 A/B blend. (The latter composition corresponds to a critical mixture, that is, the composition at the critical point in a temperature vs composition phase diagram for the binary mixture.) The radius of the particles, R_0, is set equal to 1, where all lengths are given in units of the lattice spacing a. (Although the simulation can accommodate relatively large particles, we consider particles with the smallest possible radius in order to eliminate extraneous length scales and thus, more effectively analyze the dynamical properties of the blend.) Unless stated otherwise, the following values of the parameters were used in all the simulations: $\zeta = 1.3$, $c = 0.5$, $M = 1$, and $M_p = 1$. The noise acting on the order parameter ψ is set to zero; this choice will not significantly affect the long-time behavior of the fluids. Here, the coupling constant C (eq 4) is also set to zero. In the initial configuration of the system, the particles are randomly dispersed, and the initial fluctuations of ψ are Gaussian with a variance of 0.05. Each system was run for 20000 to 100000 time steps, and the data were averaged over three to five runs.

To illustrate the dramatic effect that the mobile particles have on the morphology of the system, we first compare the structures in the absence (Figure 2a) and presence (Figure 2b) of these fillers. As can be seen in Figure 2a, the particle-free system forms a bicontinuous pattern, which is typical of a mixture undergoing spinodal decomposition. On the other hand, with the addition of just 100 A-coated particles (a three percent volume fraction), the bicontinuous structure is destroyed, and we now observe islands of B in a continuous sea of A.[22]

The above patterns represent the late-stage structure. By examining the morphologies as a function of time, we can obtain insight into the factors that contribute to these shapes. Figure 3a captures the early-time behavior of the mixture. What is striking is the fact that the particles nucleate spherical A-rich domains, which are encircled by layers of B-rich phase. The particles act as heterogeneous nucleation sites in the phase-separation process. Similar images have been seen experimentally by Karim et al.[9a] at early times in a film of two immiscible polymers and immobile silica beads, which are wetted by one of the polymers. Simulations for phase-separating binary mixtures in the presence of immobile spheres also show this pattern.[7d,23] At intermediate times (Figure 3b), we see the incipient disruption of the B network. As the coated particles diffuse to a new location, the compatible A fluid engulfs these particles; this process effectively cuts the B domains. Further coarsening of B-domains is inhibited by the A-coated particles acting as obstacles to the motion of interfaces. This is clear from the late-stage morphology seen in Figure 2b.

To quantify our observations on the evolution of the domains, we calculate the characteristic domain size as a function of time for various number of particles. One measure of the characteristic size is given by the "broken bonds" formula for the inverse "area" density, $R \sim L^d/A(t)$, where L^d is the "volume" of the system, and $A(t)$ is the total "area" of the interface.[20] For a two-dimensional system, we can introduce two characteristic lengths $R_x = L^2/N_x$ and $R_y = L^2/N_y$, where N_x and N_y are the numbers of "broken bonds" (pairs of nearest neighbor sites with opposite signs of ψ) in the x and y directions, respectively. The isotropic measure of the characteristic domain size ($1/R \sim 1/R_x + 1/R_y$) gives the same asymptotic behavior as that calculated from the correlation or scattering functions in ordinary spinodal decomposition.

Figure 4a shows the plot of $R(t)$ versus t for different numbers of particles, N. In the absence of particles ($N = 0$), the growth of the domains obeys the Lifshitz−Slyozov law, with $R(t)$ scaling as $t^{1/3}$. With the addition of particles, the initial domain

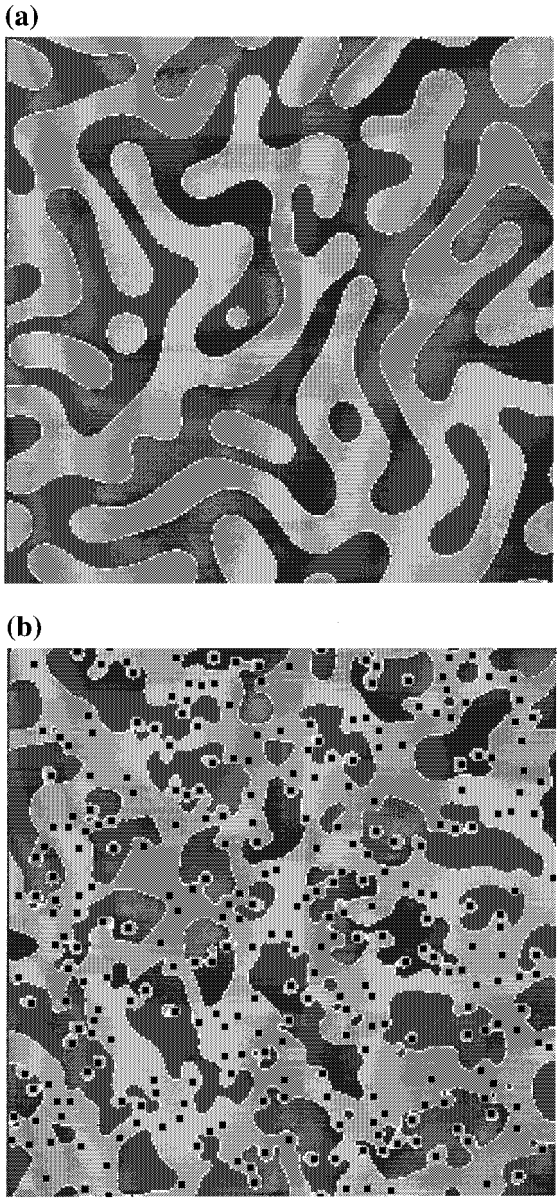

Figure 2. Graphical output from the simulation for the case of no particles ($N = 0$) in (a), and $N = 300$ particles in (b). The lighter domains are fluid A, the darker domains are fluid B, and the white regions are interfaces. In (b), the dark circles are the particles. The particles are wet by the A phase. The images represent the late-stage morphology. Images similar to 2b are also seen for $N = 100$.

growth (early stages of phase separation) still satisfies the Lifshitz−Slyozov law, but there is a density-dependent amplitude $E(n)$ that depends smoothly on the particle density, $n = N/L^2$. In particular, for sufficiently low particle density, we find $R(t) \sim E(n)t^{1/3}$, where $E(n) = E_0(1 + \alpha n)$, with $E_0 \approx 0.4$ being the growth prefactor in a particle-free system, and $\alpha = 13.1$. (We note that the factor $E(n)$ only modifies the amplitude of the curve, but does not affect the growth law.) This growth continues until the characteristic domain size becomes comparable to the average interparticle distance $n^{-1/d}$. At that point, the wetting phase (A) percolates to form a single infinite domain, and droplets of the B phase are trapped inside this domain (Figure 3b). Now for $N \geq 100$, the presence of particles slows down the domain growth, as can be seen for late times in Figure 4a. The slower domain growth and the altered structures (Figure 2b) are qualitatively similar to the observations of Tanaka et al.[8]

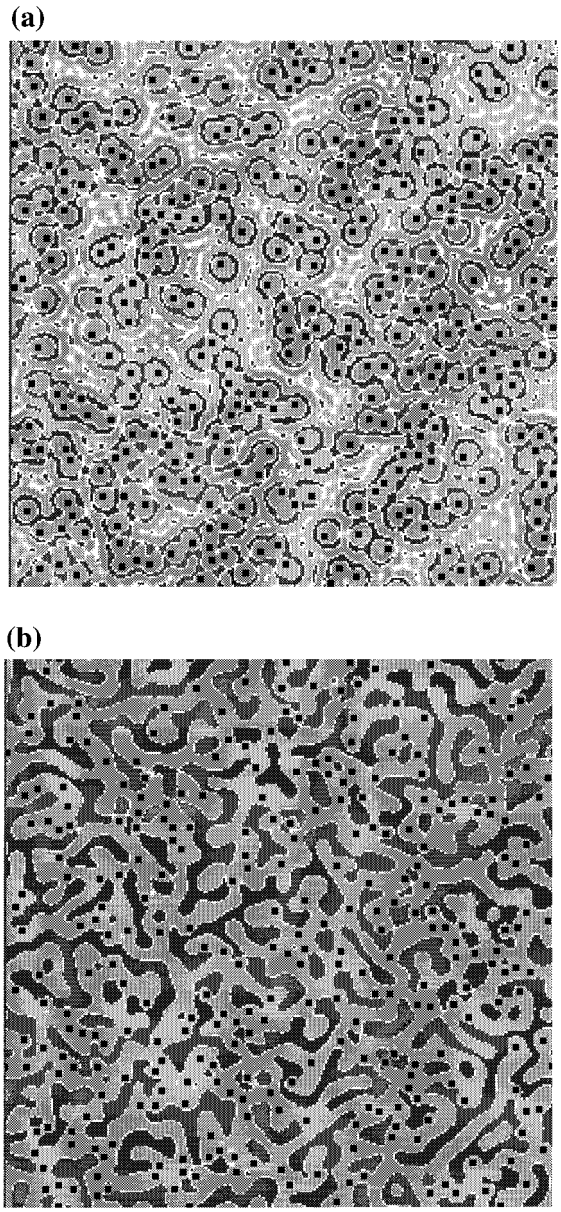

Figure 3. (a) Early-time behavior of the mixture where the particles act as nucleating sites in the phase-separation process. Initially, the system is in the mixed state; throughout the lattice, $\psi \approx 0$, which corresponds to the white regions. After a short time, the A-rich and B-rich regions begin to form. (b) At intermediate times, the B network is disrupted by the mobile, A-coated particles. Here $N = 300$. Similar images are also seen for $N = 100$.

To capture the dependence of the characteristic size on both time and the particle density, we propose the following dynamical scaling function,

$$R(t) = n^{-1/2}\,(1 + \alpha n)\,G(btn^{\gamma/2}) \qquad (14)$$

where $b \approx 1$, $G(x)$ behaves as $G(x) \approx G_0 x^{1/3}$ for small x ($b^{1/3}G_0 = E_0$), and $\gamma = 3$ (which is required to satisfy the transition to the Lifshitz−Slyozov growth law for $n \rightarrow 0$). As Figure 4a indicates, there is clearly a slowing of growth at large time, and for large x, it is reasonable to assume $G(x) \sim x^{\delta}$ with a small power δ (or even logarithmic growth). A similar scaling function was used by Gyure et al.[24] to describe the dependence of the domain growth on the number of impurities in a time-dependent Ginzburg−Landau model. We introduced the additional factor $(1 + \alpha n)$ to account for the effective off-criticality

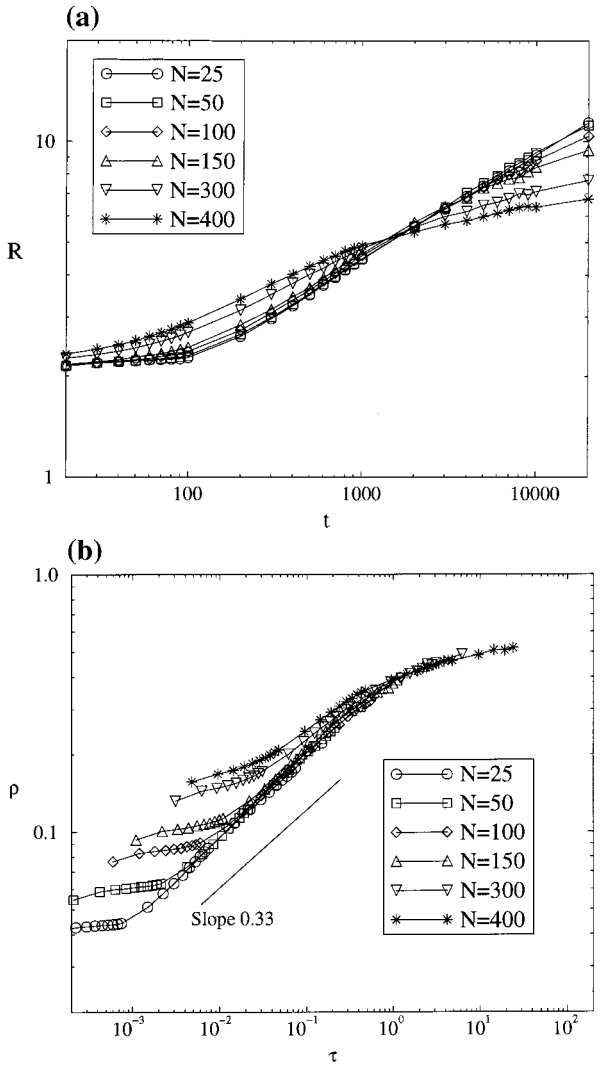

Figure 4. Characteristic length as a function of time: (a) unscaled R vs t, and (b) scaled coordinates $\rho = Rn^{1/2}/(1 + \alpha n)$ vs $\tau = tn^{3/2}$, where $n = N/L^2$. The data are averaged over 3 independent runs. The growth exponent $\nu \sim 1/3$ in the early time range $10^{-2} < \tau < 10^{0}$.

induced by particles. To illustrate this scaling behavior, we plot the characteristic size in scaled coordinates $\rho = R(t)n^{1/2}/(1 + \alpha n)$ vs $\tau = tn^{3/2}$ in Figure 4b. For $\alpha = 13.1$, it can be seen that all data fit reasonably well onto one master curve, with the exception of the $N = 400$ case, where additional n-dependence is presumably required.

The observed slowing down of the domain growth is reminiscent of the interface pinning in Ising-type systems with quenched impurities.[24−27] In the latter studies, impurities reduced the local interfacial tension and thus enforced late-time pinning, with domain growth slowing down logarithmically, $R \sim (\ln t)^{\eta}$. A similar effect was also seen in the "hybrid" model of Kawakatsu et al.[11] for a binary mixture with surfactant molecules. On the other hand, our hard particles, which do not behave as surfactants and are preferred by the A phase, slow the domain growth by acting as obstacles to the interface motion. When the characteristic domain size becomes comparable to the interparticle distance, interface coarsening becomes hindered by these obstacles, and the slowing down occurs.[28] It is likely that at the very late stage, the domain growth would stop completely (as indicated by the behavior of the $N = 400$ curve).

We can determine the long-time asymptotic behavior of the system by turning to our analytic model. As noted in the Models section, we can calculate the steady-state domain size, R* from

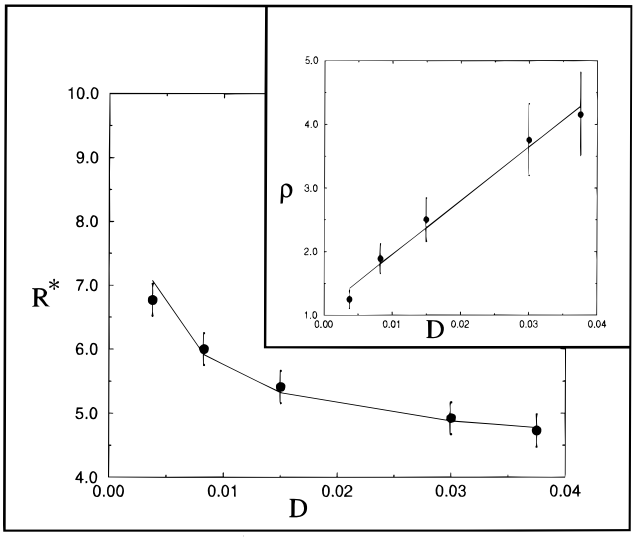

Figure 5. Final domain size R^* vs diffusion constant D for the $N = 600$ system: (a) linear scale, and (b) scaled coordinates $\rho = (R^{*3}D)$ vs D. Solid line represents the best fit, $\rho = (R^{*3}D) = 1.05 + 4.80D$. The points are the data from the simulation, and the vertical lines are the error bars. The simulation data is averaged over 3 independent runs.

the fixed point of the kinetic equations. We find that

$$n_-^* = k_1 n/(k_2 + k_1 + k_{-1}) \tag{15}$$

and

$$R^* = 1/\sigma^* = (A/k_2 l n_-^*)^{1/3} = (\mathrm{A}(k_2 + k_1 + k_{-1})/k_1 k_2 \mathrm{n}\, l)^{1/3} \tag{16}$$

The existence of a fixed point that can be reached in the physical quadrant $R > 0$, $n \geq 0$ indicates saturation in this mean-field analysis.

By postulating the dependence of k_1, k_{-1}, and k_2 on D, the diffusion constant for the particles, we can obtain a relationship between R^*, n, and D. We argue that both k_1 and k_{-1} must be proportional to D because they are directly related to the "hopping probability" of particles near interfaces. On the other hand, k_2 has a contribution from the motion of an interface segment near a stationary particle, and thus, can be considered D-independent (at least, to a first approximation). With this in mind, we obtain,

$$R^* \sim (A/Dn)^{1/3} (1 + \beta D)^{1/3} \tag{17}$$

where the constant $\beta \sim R_0/A$, and R_0 is the radius of the particle. To test this prediction and the adequacy of the rate equations, we performed a set of simulations for $N = 600$ for different values of D. The results showed good agreement between the simulation data and the theory (see Figure 5), with a plot of $(R^*)^3D$ vs D yielding a straight line (as shown in in the inset), confirming the prediction in eq 17.

The expectation from eq 17 is that R^* decreases when either the particle density or the diffusion constant are increased. For large D ($D \gg \beta^{-1}$), R^* is D-independent, while for small D ($D < \beta^{-1}$), R^* is proportional to $D^{-1/3}$. Note that for very small D, the model must break down. Indeed, once the characteristic size R^* becomes comparable to the interparticle distance $\mathrm{n}^{-1/2}$, we can no longer neglect multiparticle processes (e.g., involving higher powers of n). For such systems, interface pinning would presumably occur at $R' \sim n^{-1/2}$, pre-empting the saturation described by the current theory. This condition imposes a lower

bound on the diffusion constant: $D > An^{1/2}$. Below this value, the final domain size is D-independent and scales such as $n^{-1/2}$. Thus, the final domain size depends on D in the region $An^{1/2} < D < A/R_0$. In this region, $R^* \sim D^{-1/3}$, while for $D \gg A/R_0$, R^* is almost D-independent.

The dependence of the final domain size on the particle concentration is also interesting. We find that for $D = 0$ (immobile particles), the final domain size is proportional to $n^{-1/2}$.[23] This result is presumably due to the fact that when the particles are immobile, the only relevant length scale is the interparticle distance $n^{-1/2}$. For nonzero D, there is a crossover between the "geometric" pinning $R' \sim n^{-1/2}$ and the "kinetic" steady-state size $R^* \sim (A/Dn)^{1/3}$. This crossover occurs near the particle concentration $n' \sim (D/A)^2$: when $n \gg n'$, the characteristic length is D-independent and scales as $n^{-1/2}$; when $n \ll n'$, the characteristic length scales as $(Dn)^{-1/3}$.

Our results on the dependence of the final domain size on the diffusion constant show qualitative agreement with earlier findings of Srolovitz and Hassold,[27] who performed dynamical Monte Carlo simulations of a nonconserved Ising model with diffusing, surfactant-like point particles. They also found that an increase in defect mobility leads to a decrease in the final domain size.

To elucidate the importance of wetting on the observed slowing down of the domain growth, we performed a simulation with hard, mobile particles and no preferential adsorption (in other words, they are neutral to both A and B). The following boundary conditions are applied on the surface of the particles: $\partial_n\psi(\mathbf{r}, t) = 0$, $\partial_n F(\mathbf{r}, t) = 0$. For $N = 300$ particles and no wetting, we observed no deviation from the Lifshitz−Slyozov growth law within the time scale of our simulations ((20 000 time steps). (In this case, the particles are randomly distributed throughout the film; they are equally likely to be in the A phase as in the B phase.) This result indicates that the slowing down is clearly enhanced by the strong wetting and not merely by the effects of excluded volume or particle mobility. Indeed, in these simulations (without coupling between the particles and ψ) nonwetting particles neither pin nor block interfaces, and thus, have only minimal effect on the dynamics of the late-stage coarsening.

In the above studies, we have neglected interactions among the particles. Such interactions can, however, dramatically alter the previously observed growth behavior and morphology of the mixture. Consider the illustrative examples in Figure 6a,b; we have introduced a Lennard−Jones attraction in the first case and a screened, $1/r$ repulsion in the second. In the case of *attractive* interactions, the particles can aggregate into distinct clusters. Because the clusters are localized in space, there is effectively more room for the growth of B domains. Thus, the B domains are larger in size (Figure 6a) than in the case of no interparticle attraction (Figure 2b). Indeed, instead of "freezing", we again find that $R \sim t^{1/3}$ (over the time range considered in the simulation). On the other hand, a screened electrostatic *repulsion* between the particles gives rise to a relatively uniform distribution of solid filler particles throughout the mixture (Figure 6b). The regularly dispersed particles pin the B fluid into domains that are smaller than those in Figure 2b (the no interaction case, where fluctuations in the positions of the particles can give rise to some large B regions). Thus, the plot of R vs t for the case of electrostatic repulsion shows the slowest growth behavior. For either attractive or repulsive interactions, the simulations reveal a more regular distribution in the size and shape of the B domains than in the case of no interactions. This can already be seen by comparing Figures 2b and 6.

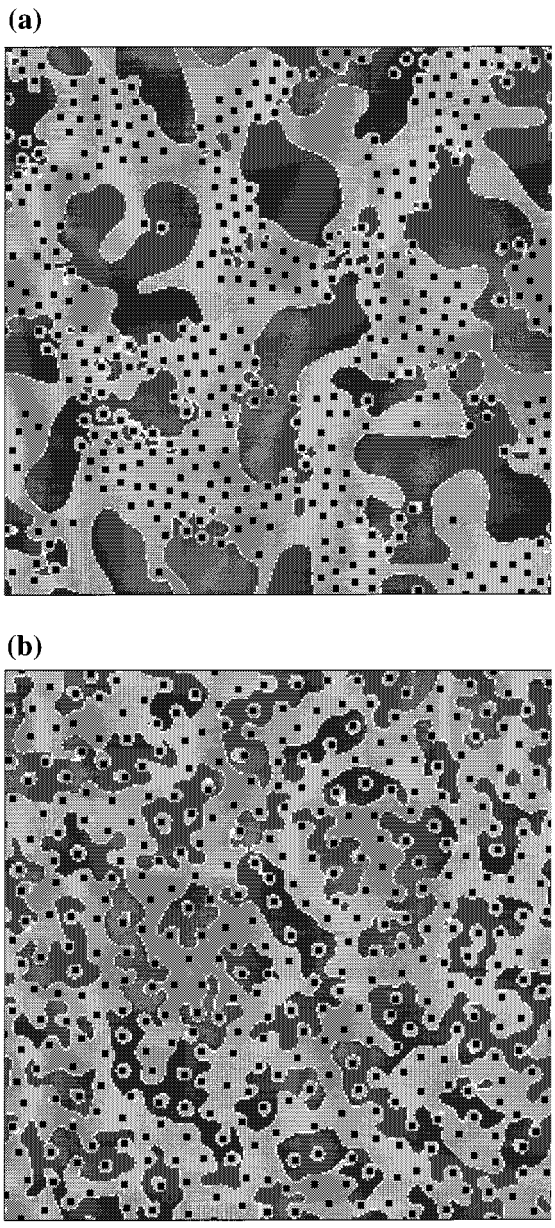

Figure 6. In (a), the particles interact through a screened electrostatic repulsion, and in (b) the particles interact through a Lennard−Jones attraction. In both cases, $N = 400$ and $t = 30000$ time steps.

Through the above calculations, we see that even a small volume fraction of such nanoscopic particles strongly modifies the domain growth and the final morphology of the system relative to the no-particle case. We also see that varying the particle number density, mobility, wetting behavior, and interparticle interactions provides a means of tailoring the structure of the system. Since the structure plays a crucial role in dictating the macroscopic behavior, the results are useful for controlling the properties of the material. Another factor that plays an important role in the ultimate structure and properties of the composite is the processing conditions. In the processing of polymeric mixtures, the system is typically subjected to shear in order to promote greater intermixing of the different components. In the calculations described below, we investigate the behavior of the system under shear.

Mixture under Shear. By applying eqs 7−9, we model the phase separation under shear of the binary 50:50 mixture and hard particles.[18] In this model, we neglect hydrodynamic interactions and assume that the shear is externally imposed.

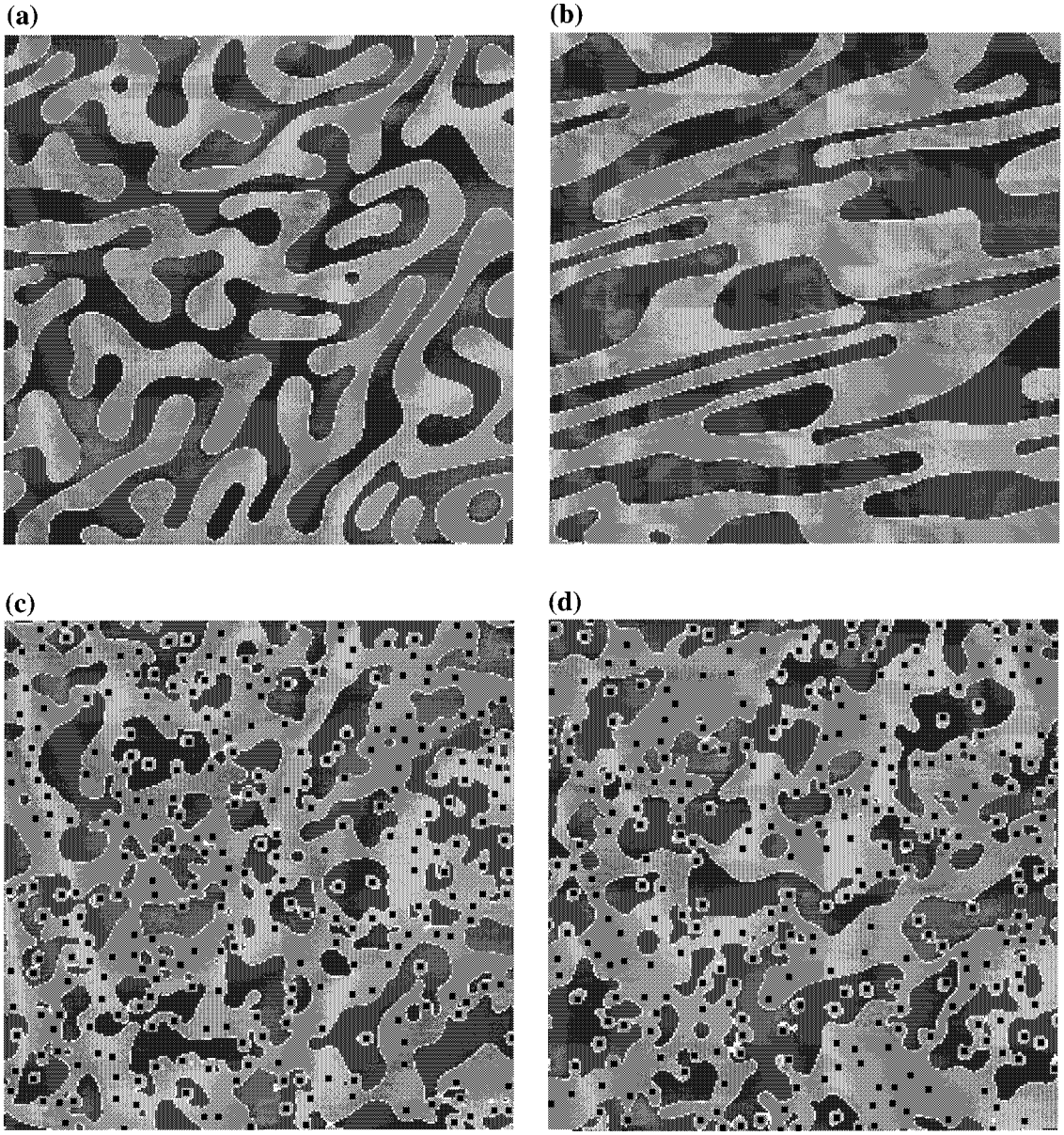

Figure 7. Morphology of the mixture under shear for $S = 1 \times 10^{-4}$ and (a) $N = 0$, $\gamma = 1$; (b) $N = 0$, $\gamma = 5$; (c) $N = 300$, $\gamma = 1$; (d) $N = 300$, $\gamma = 5$. Black circles represent particles, light gray regions are the A-phase domains, dark gray regions are the B-phase domains, and white points are interfaces. As the figures show, increasing the shear strain for the particle-free system changes the morphology from relatively isotropic in (a) to anisotropic in (b). In the case of $N = 300$ particles, however, the domains remain relatively isotropic at both the lower (c) and higher (d) shear strains.

The advection (shear) direction is along the horizontal (x-) axis. The shear rate S was varied by a factor of 5, from 1×10^{-4} to 5×10^{-4}. (For shear rates higher than 5×10^{-4}, numerical instabilities occur in the present calculation scheme, while for shear rates lower than 1×10^{-4}, the time required to observe significant changes in morphology becomes too large.) We define the shear strain as $\gamma = St$, where t is the number of time steps. In each time step, the value of ψ and the position of each particle is updated once. (By describing our results in terms of the dimensionless quantity γ, rather than in units of time steps, we facilitate comparison with eventual experimental studies.) The shear strain was restricted $\gamma \leq \gamma_{max} = 5$ to avoid finite size effects. The size of the lattice for the results described below was 256×256 sites. Runs were also carried out on lattices of 128×128 and 512×512 sites as a practical way to ensure the absence of finite size effects.

Once again the figures provide insight into the behavior of the system and the effect of the particles on the structure of the mixture. As a basis of comparison, we first consider the characteristics of the particle-free blend. For $\gamma \leq 1$ and in the absence of particles ($N = 0$), the domains grow isotropically (Figure 7a), which is typical of normal spinodal decomposition. At the largest shear strain ($\gamma = 5$), the structure is modified significantly by the applied flow, with domains being deformed and aligned along the shear (x-) direction (Figure 7b). When a small number of particles (i.e., $N = 50$) is added to the mixture, the morphologies are relatively unaffected for both $\gamma = 1$ and 5. At $N = 100$, however, the structure no longer resembles a bicontinuous network.[18] The stripe-like B domains have been effectively "cut" by the mobile particles.[29] The A coating around the particles promotes the percolation of A domains, and thus hinders the growth and limits the size of the B regions. Nonetheless, the domains remain anisotropic in shape. Further increases in the number of particles, however, give rise to dramatic and systematic changes in the structure of the mixture, as illustrated by the $N = 300$ example in Figures 7c,d. For both γ

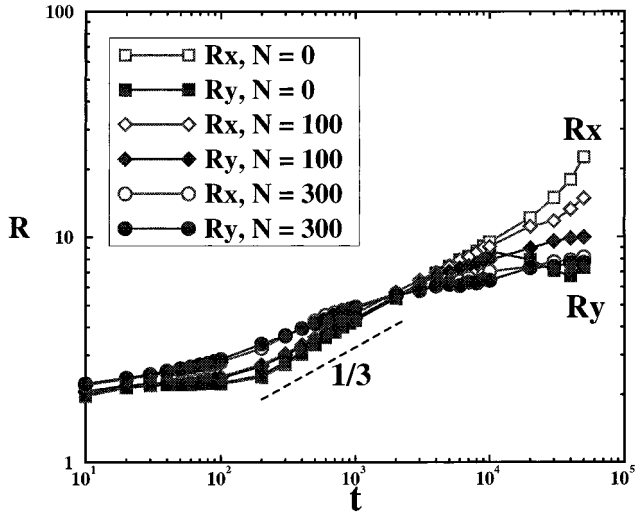

Figure 8. Time evolution of the characteristic domain size along (R_x) and perpendicular (R_y) to the shear direction for $S = 1 \times 10^{-4}$ and different particle densities.

$= 1$ and 5 at $N = 300$, the domains now appear isotropic in shape.

To quantify our observations on the shape of the evolving domains, we again use the "broken bond" formula to calculate the characteristic sizes along (R_x) and perpendicular (R_y) to the shear direction. The time evolution of these characteristic sizes for $N = 0$, 100, and 300 is shown in Figure 8. From this plot, we can see that the particles influence the system in two specific ways. First, at late stages, the fillers slow the growth in the shear direction relative to the $N = 0$ case. Second, as the number of particles is increased, R_x approaches the value of R_y until at $N = 300$, $R_x \approx R_y$. Thus, it appears that for some critical N_c, the particles effectively promote the formation of isotropic domains. (Again, to confirm that these effects are due to the particles and not the effective off-criticality of the system, we ran simulations for 53:47 and 55:45 AB blends under shear in the absence of particles. In these cases, the evolution of R_x and R_y is comparable to that for the 50:50 no-particle ($N = 0$) case. This indicates that it is the mobile particles that are responsible for the observed changes in domain growth and morphology.)

We can obtain further insight into the anisotropy of the growth by plotting $[R_y(t)/R_x(t)]$ as a function of time for different N and shear rates, S. We first focus on the regime of relatively low particle numbers, or as we will see, $N < N_c$; plots of these data are shown in Figure 9. The domain growth rate is initially much larger than the domain deformation rate, and thus at early times, the domains are not significantly deformed by the shear flow. At this stage, the growth is consistent with $R_x \approx R_y \sim t^{1/3}$. This Lifshitz−Slyozov (LS) growth continues until the point where the rate at which the domains are being deformed by the shear (Γ_S) exceeds the isotropic LS growth rate (Γ_{LS}). We approximate the domain deformation rate as $\Gamma_S \approx S_e = S(1 - \beta n/S)$, where n is the particle number density, $n = N/L^2$, and β is a positive parameter.[30] The Γ_{LS} growth rate is given by $(1/R(t))(dR(t)/dt) \approx 1/3(t^{-1})$. By equating Γ_S and Γ_{LS}, we can obtain a crossover time $t^* \approx S_e^{-1}$. After this crossover time, the domains grow much faster along the shear direction, while they essentially stop growing in the perpendicular direction. Then, R_y saturates and it is reasonable to assume that R_x grows at late time as t^α with $\alpha = 1$ (because at late-stages the shear induces an affine deformation[31]).

Using the above arguments, we suggest the following scaling function to describe the dependence of the characteristic size

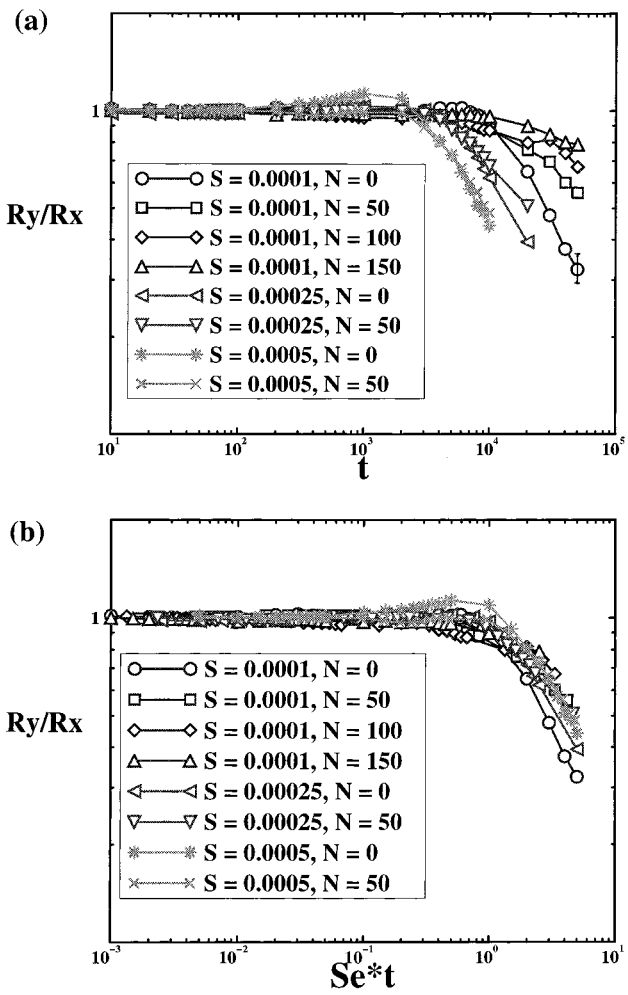

Figure 9. (a) log−log plot of $R_y(t)/R_x(t)$ vs time for different shear rates and particle densities. The standard deviation for the data is ± 10%. This is marked for the $N = 0$, $S = 1 \times 10^{-4}$ case; for the other cases, the error bars are comparable to the size of the symbols. (b) log−log plot of $R_y(t)/R_x(t)$ vs tSe, where $Se = S(1 - \beta n/S)$, $n = N/L^2$, and $\beta = 0.022$.

on the time, shear rate, and particle density (for sufficiently low particle density $n \ll n_c = N_c/L^2$):

$$R_y(t)/R_x(t) = G(tS_e) \tag{18}$$

The scaling function $G(z)$ behaves as $G(z) \propto$ constant, for $z \ll 1$, while for $z \gg 1$, $G(z) \propto z^{-\alpha}$, where $\alpha \approx 1$ since, as noted, the shear produces affine deformations of the domains. The scaling results are shown in Figure 9b; the data collapse reasonably well with one adjustable parameter, $\beta = 0.022$. (The simulations reveal a number close to 1 for α, but we are not yet in the asymptotic regime.)

We now focus our attention on higher particle number densities ($N = 300$, 400, 600 with $S = 1 \times 10^{-4}$, and $N = 750$ with $S = 2.5 \times 10^{-4}$). As can be seen from Figure 10, domain growth along the shear and perpendicular directions is essentially the same, indicating that even under relatively large shear strain ($\gamma = 5$), the system is isotropic (see the morphology of the system with $N = 300$, $S = 1 \times 10^{-4}$ in Figure 7d). In the absence of particles at the same shear rate and strain, the system is highly anisotropic (Figure 7b). As noted above, A-coated particles that lie within B regions can propagate A domains. The growth of the A phase effectively "cuts" or breaks up the B regions. It should be noted that at late times, the characteristic

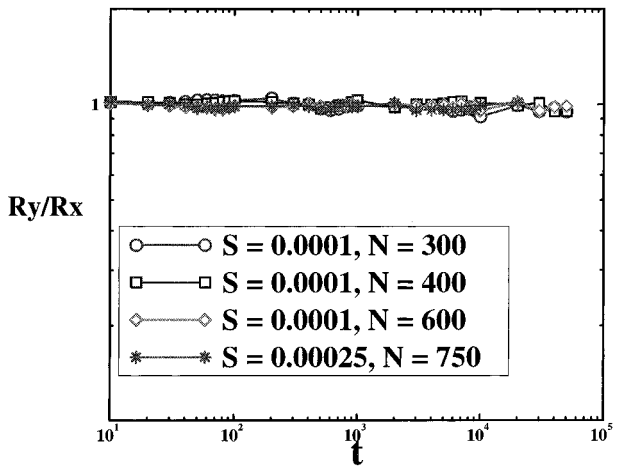

Figure 10. log−log plot of $R_y(t)/R_x(t)$ vs time for high particle number $N = 300$, 400, 600, 750, and low shear $S = 1 \times 10^{-4}$, 2.5×10^{-4}, in all cases shown to be below $S_c(n)$.

sizes are saturated in both the x and y directions. We expect that the saturated or slow domain growth will persist to even larger shear strains.

Finally, we can estimate the critical shear rate at which the domains change shape from anisotropic to isotropic. Since this change occurs at a relatively late stage, the Lifshitz−Slyozov growth mechanism can be neglected. The following argument for the transition point is based on a competition between the deforming effect of the shear flow and the "cutting" effect of the diffusing particles. First, we estimate the domain growth rate, Γ_P, due to the "cutting" effect. The following argument is given for 2D to correspond to the simulations. If a particle moves one lattice site from the wetting phase to the nonwetting phase, it will create new interfaces of length a on two "edges" of the particle. Thus, for a $L \times L$ system within one time step, the increase in interface, ΔA, due to the random jumping of the particles is given by $\Delta A \sim aNP_I p(a)$. Here, P_I is the probability that a particle borders an interface and $p(a)$ is the probability that the particle moves one lattice site, a, (in the right direction) in one time step Δt. In the late stage of anisotropic growth, the domains basically form long, interconnected stripes with characteristic lengths R_x and $A_x = L^2/R_x$. Thus, P_I can be estimated as a/R_x. Since the particles are randomly moving on the lattice, $p(a)$ is estimated as $p(a) = D_p/a^2$, where D_p is the diffusion constant of the particles (and in our model is equal to $G^2/2$, where G is the amplitude of the noise acting on the particle).

The domain growth rate due to the random motion of the particles can be calculated using the formula for the broken bonds, or $\Gamma_P = [L^2/(A_x + \Delta A_x) - L^2/A_x]/R_x \approx -R_x \Delta A_x/L^2$. Using the expression for ΔA, we finally obtain, $\Gamma_P \approx -(N/L^2)D_p$, where we have set $a = 1$. Since the deformation rate of the domains under shear is $\Gamma_S \approx S$, we can find the critical value for S as

$$S_c \sim nD_p \tag{19}$$

For the parameters in our system ($N = 300$ and $D_p = 0.05$), $S_c \approx 10^{-4}$; thus, for the case with shear rate $S = 5 \times 10^{-4}$, it appears that $S > S_c$, and we would expect anisotropic domain growth, while for $S = 1 \times 10^{-4}$, an isotropic morphology is suggested. Both conclusions are in agreement with the simulation results. We emphasize that the important physics in eq 19 is that the critical shear rate S_c suggested by these arguments is linearly proportional to the particle number density. (We note that eq 19 is also valid in 3D if the same mechanisms prevail.)

In our studies of the mixture under shear, we also examined the case where C, the coupling constant in eq 4, is set to a small finite value (the magnitude of M_p $(-\partial H_{CPL}/\partial \mathbf{R}_i)$ is small compared to the magnitude of the noise term). Thus, the fluid now influences the motion of the particles. The above conclusions are still valid for small values of C. (For larger values of C, similar results can be obtained by increasing the noise acting on the particle, since this effectively increases the mobility of the filler. See eqs 4 and 5.)

Equation 19 provides a useful prescription for optimizing the processing of the system, and the properties of the material. Namely, for a fixed particle concentration, one can modify the shear rate, or for a fixed shear rate, one can control the particle concentration ($n_c \sim S/D_p$) to create isotropic domains. The composite is more intermixed in the case of the more isotropic domains; consequently, the material can exhibit greater strength and structural integrity.

Up to this point, we have not explicitly taken into account the polymeric nature of the components forming the binary mixture. In the following section, we show how the computer model can be adapted to incorporate diblock copolymers. One motivation for considering mixtures of diblocks and particles is their potential use in fabricating novel electronic or optical devices. The attractive feature of AB diblocks is that they can microsegregate into lamellar layers or spherical domains (and even more complicated patterns), which are tens of nanometers is size. If A and B are chosen so that a metallic compound preferentially wets one of the stripes, metal can be vapor deposited onto the polymer substrate in a highly controlled manner.[32,33] This system of alternating polymeric and metallic domains, whose features are an order of magnitude smaller than typically achieved through photolithography, should exhibit unique optical or electronic properties. Below, we use our computational model to investigate the structural properties of these systems.

Diblocks and Fillers. To model the dynamics of microphase separation in a melt of diblock copolymers, we modify eq 1 to read[34]

$$\partial\psi/\partial t = M\nabla^2(\delta H\{\psi\}/\delta\psi) - \Gamma(\psi - F_0) + \xi \tag{20}$$

Here, Γ is a constant, $F_0 = \langle\psi\rangle$ is the ensemble-averaged order parameter, and ξ is a conserved zero mean Gaussian noise. The term $[-\Gamma(\psi - F_0)]$ limits the growth of the fluid domains and introduces the geometric constraint relevant to the diblocks. Without this term, the fluid domains would continue to grow with time (as $R \sim t^{1/3}$). The specific size of the domains is governed by the parameter Γ, which is proportional to N^{-2}, where N is the length of the block copolymer.[35,36] Thus, eq 20 captures essential features of the microphase separation of diblocks: the polymers self-assemble into finite-sized domains whose size depends on the length of the chains. In these calculations, the value of Γ is fixed at 0.002 and we initially set the coupling constant C in eq 4 to zero. (This corresponds to the case where the particles move purely diffusely.)

Through the two-dimensional studies, we can simulate the behavior of diblock films that are similar to those studied by Morkved et al.[32,33] In these studies, the films appear as if one of the blocks were "decorated" by the metal particles. The driving force for this type of self-assembly is a selective interaction between the particles and one of the polymeric components. In our simulation, the A "coating" on the surface of the particles ($\psi_s = 1$) causes the particles to be preferentially localized in the A phase. Hence, we capture the selective wetting behavior that plays a crucial role in the experimental studies.

Of particular interest is determining if and how the particles affect the structure of the underlying polymeric pattern. To address this question, we turn to Figure 11, parts a and b, which show the respective, late-stage morphologies for a film of symmetric ($F_0 = 0$) and asymmetric (30:70, $F_0 = -0.4$) AB diblocks that contain $N = 400$ particles. (The value of F_0 is set for the background fluid.) The insets in the figures show the structure of the diblocks in the absence of particles ($N = 0$). For the symmetric system and $N = 400$, the particles self-assemble in the lamellae of the A-phase. By comparing the images in Figure 11, we see that the B regions are effectively "cut" by moving particles and the morphology changes from the bicontinuous lamellar structure to the one where the A phase percolates and B phase consists of many separate elongated domains. For the asymmetric system, the particles form large clusters and help speed up the coalescence of A-phase droplets within the majority (B) phase. The patterns are in sharp contrast to the behavior of the no-particle systems seen in the insets in the figures.

The above findings indicate that the diffusing particles not only decorate the A domains, but also decrease the domain size, thereby perturbing the self-assembly of the diblocks. These conclusions hold for $C = 0$ (no coupling force), as well as small values of C. For higher values of C, the force acting on the particles from the evolving fluid diminishes the diffusive behavior of the particles. The fillers become highly localized in the A domains and are less effective at cutting the B regions. For $C = 0.1$, Figure 11c shows the late-stage morphologies for a film of symmetric diblocks that contain $N = 400$ particles. Recall that C is a measure of the strength of the interaction between the A-coated particles and the A domains. Comparison of Figure 11, parts a and c, reveals that the structure and size of the domains in diblock/particle mixtures can be controlled by tailoring the interaction between the particles and the one of the blocks in the copolymer. We note that the morphology seen in Figure 11c is very similar to that observed by Morkved et al.[32] indicating a strong wetting interaction between the particles and one of the blocks in their experimental system. We are now carrying out more systematic studies on these diblock/particle composites.[37]

Conclusions

In summary, we developed a computer simulation and a set of mean-field equations to describe the phase separation of binary blends in the presence of hard, mobile particles. The models allow us to investigate the rich behavior of solid, nanoscale colloids in complex fluids. These methods are useful for gaining insight into the physics of complex mixtures and tackling industrially important problems since polymeric formulations or coatings are typically multiphase, multicomponent systems.

In the present studies, we focused on the case where one of the fluids preferentially wets the surface of the particles. We see that even a three percent volume fraction of such nanoscopic particles strongly modifies the domain growth and the final morphology of the system relative to the no-particle case. Furthermore, the findings indicate that the intermixing between the species can be controlled by varying the number density and mobility of the particles, as well as the wetting and interparticle interactions. The extent to which the system is intermixed plays a crucial role in dictating the overall integrity and strength of the material. These theoretical results provide useful guidelines for improving the mechanical behavior of polymeric composites.

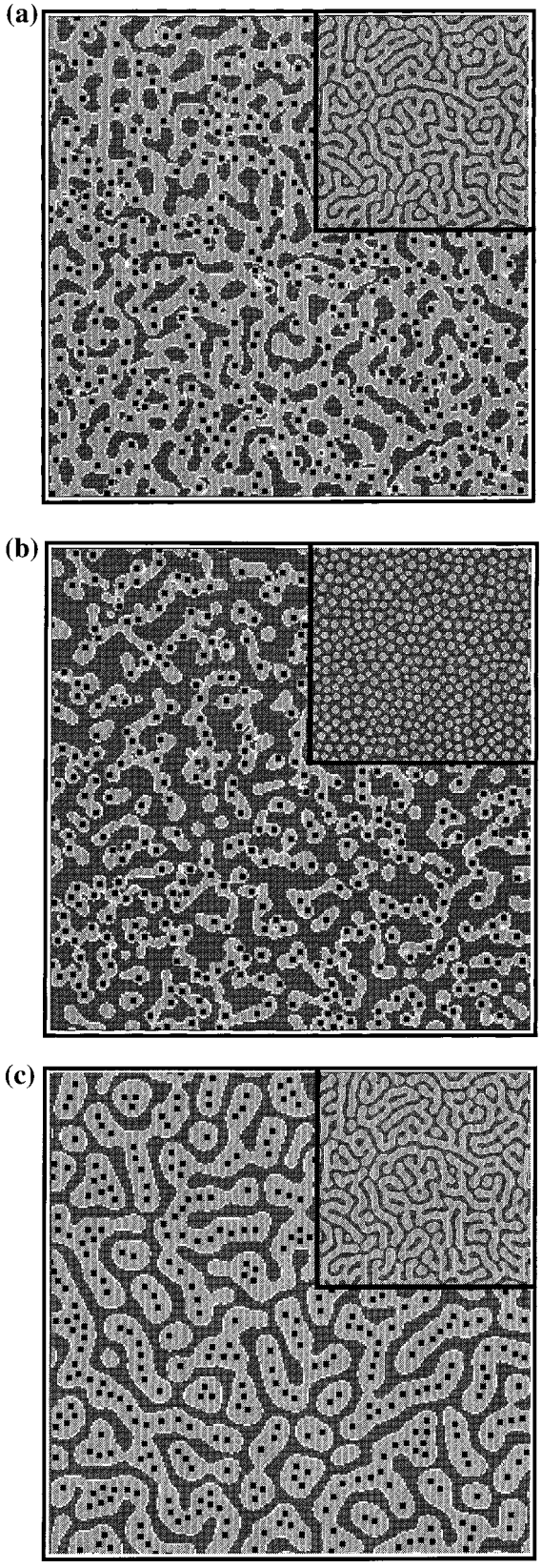

Figure 11. The pattern after 5000 time steps for various diblock copolymer systems. In (a), $N = 400$, and the copolymer is a 50:50 AB diblock. The inset shows the particle-free case ($N = 0$). In (b), $N = 400$, and the copolymer is a 30:70 diblock. The inset shows the morphology for the $N = 0$ case. In (c), $N = 400$, and the copolymer is a 50:50 AB diblock, however, the coupling interaction in eq 3 is now included and $C = 0.1$. The inset shows the morphology for the $N = 0$ case.

Processing conditions also play a critical role in shaping the morphology and the final properties of the material. For mixtures under an imposed shear, our simulations indicate that initially the domains grow in an isotropic manner and obey the Lifshitz−Slyozov "1/3 law". At later times, the domains grow faster along the shear direction and ultimately stop growing or grow extremely slowly in the perpendicular direction. For sufficiently high particle density, however, this anisotropic growth is destroyed by the randomly moving, coated particles; hence, an isotropic morphology can be observed even at large shear strain. For mobile particles, our results suggest that increasing the particle loading to n_c or greater (as can be estimated from eq 19) promotes greater intermixing between the A and B phases. These findings provide additional routes for improving the mechanical properties of nanocomposites.

We also adapted our computer model to describe the role of hard mobile particles in the microphase separation of AB diblock copolymers. The particles are wet by and thus have a selective interaction with the A blocks. As observed in the experimental results, the particles become localized in the A domains. We find, however, that the particles not only decorate the A domains, but also affect the morphology of the polymeric pattern. We are now systematically examining how the number and strength of particle-block interactions affects the overall structure of the film.[37]

In all the above studies, we restricted our consideration to spherical particles. The model can be modified to describe rodlike particles, such as nanotubes, or mixtures of rods and spheres. Studies are currently underway on the role that filler architecture plays in the morphology of the mixture. Altering the size, shape, or aspect ratio of the particles may provide another means of tailoring the microstructure, and hence macroscopic behavior, of polymeric composites. Finally, we note that in the computations described here, we have not taken into account hydrodynamic interactions or differences in the viscosities of the two fluids. In addition, we have not considered the viscoelastic behavior of the polymers. Our model, however, provides a powerful framework for introducing these various effects and determining how they influence the behavior of the system. These investigations will be the subject of future studies.

Acknowledgment. D.J. gratefully acknowledges financial support from the NSF, through Grant DMR9217935. D.J. and A.C.B. gratefully acknowledge support from the Army Office of Research. A.C.B. gratefully acknowledges NSF, through Grant DMR9709101, DOE, through Grant DE-FG02-90ER45438 and ONR, through grant N00014-91-J-1363.

References and Notes

(1) Van Oene, H. In *Polymer Blends*; Paul, D. R., Newman, S., Eds.; Academic Press: Orlando, 1978; Vol. 1, Chapter 7.

(2) (a) Utracki, L. A. *Polymer Alloys and Blends*; Hansen Publishers: Munich, 1989. (b) Paul, D. R. In *Polymer Blends*; Paul, D. R., Newman, S., Eds.; Academic Press: New York, 1978; Vol. 2, Chapter 12.

(3) (a) Kojima, Y.; Usuki, A.; Kawasumi, M.; Okada, A.; Kurauchi, T.; Kamigaito, O. *J. Polym. Sci.: Part A: Polym. Chem*. **1993**, *31*, 983. (b) Krishnamoorti, R.; Vaia, R. A.; Giannelis, E. P. *Chem. Mater*. **1996**, *8*, 1728.

(4) Yano, K.; Uzuki, A.; Okada, A.; Kurauchi, T.; Kamigaito, O. *J. Polym. Sci.: Part A: Polym. Chem*. **1993**, *31*, 2493.

(5) (a) Fried, J. *Polymer Science and Technology*; Prentice Hall: New York, 1995; Chapter 7. (b) McCrum, N. G.; Buckley, C. P.; Bucknall, C. B. *Principles of Polymer Engineering*; Oxford University Press: Oxford, 1997; Chapters 5 and 6.

(6) (a) Gunton, J. D.; San Miguel, M.; Sahni, P. In *Phase Transition and Critical Phenomena*; Domb, C., Lebowitz, J. L., Eds.; Academic Press: London, 1983; Vol. 8, and references therein. (b) Elder, K. R.; Rogers, T. M.; Desai, R. C. *Phys. Rev. B* **1988**, *38*, 4725. (c) Bray, A. J. *Adv. Phys.* **1994**, *43*, 357.

(7) (a) Puri, S.; Frisch, H. L. *J. Phys. Condens. Matter* **1997**, *9*, 2109. (b) Jones, R. A. L.; Norton, L. J.; Kramer, E. J.; Bates, F. S.; Wiltzius, P. *Phys. Rev. Lett*. **1991**, *66*, 1326. (c) Xie, R.; Karim, A.; Douglas, J. F.; Han, C. C.; Weiss, R. A. *Phys. Rev. Lett*. **1998**, *81*, 1251. (d) Lee, B. P.; Douglas, J.; Glotzer, S. C. *PRE* **1999**, *60*, 5812. (e)Chakrabarti, A. *J. Chem. Phys*. **1999**, *111*, 9418.

(8) Tanaka, H.; Lovinger, A. J.; Davis, D. D. *Phys. Rev. Lett*. **1994**, *72*, 2581.

(9) (a) Karim, A.; Douglas, J. F.; Nisato, G.; Liu, D. W.; Amis, E. *Macromolecules* **1999**, *32* (2), 5917. (b) Karim, A., private communication.

(10) Ginzburg, V. V.; Qiu, F.; Paniconi, M.; Peng, G.; Jasnow, D.; Balazs, A. C. *Phys. Rev. Lett*. **1999**, *82*, 4026.

(11) (a) Kawakatsu, T.; Kawasaki, K. *Physica A* **1990**, *167*, 690. (b) Kawakatsu, T.; Kawasaki, K.; Furusaka, M.; Okabayashi, H.; Kanaya, T. *J. Phys. Condens. Matt*. **1994**, *6*, 6385.

(12) (a) Laradji, M.; Guo, H.; Grant, M.; Zuckerman, M. *J. Phys. A* **1991**, *24*, L629; Laradji, M.; Guo, H.; Grant, M.; Zuckerman, M. *J. Adv. Chem. Phys*. **1995**, *89*, 159. (b) Komura, S.; Kodama, H. *Phys. Rev. E* **1997**, *55*, 1722.

(13) Ginzburg, V. V.; Peng, G.; Qiu, F.; Jasnow, D.; Balazs, A. C. *Phys. Rev. E*. **1999**, *60*, 4352.

(14) Ohta, T.; Enomoto, Y.; Harden, J.; Doi, M. *Macromolecules* **1993**, *26*, 4928.

(15) (a) Cahn, J. W.; Hilliard, J. E. *J. Chem. Phys*. **1958**, *28*, 258. (b) Cahn, J. W.; Hilliard, J. E. *J. Chem. Phys*. **1959**, *31*, 688. (c) Cahn, J. W. *Acta Metall*. **1961**, *9*, 795. (d) Cahn, J. W. *Acta Metall*. **1966**, *14*, 1685. (f) Cook, H. E. *Acta Metall*. **1970**, *18*, 297.

(16) (a) Oono, Y.; Puri, S., *Phys. Rev. A* **1988**, *38*, 434. (b) Puri, S.; Oono, Y. *Phys. Rev. A* **1988**, *38*, 1542.

(17) Ohta, T.; Nozaki, H.; Doi, M. *J. Chem. Phys*. **1990**, *93*, 2664.

(18) Qiu, F.; Ginzburg, V. V.; Paniconi, M.; Peng, G.; Jasnow, D.; Balazs, A. C. *Langmuir* **1999**, *15*, 4952.

(19) Bahiana, M.; Oono, Y. *Phys. Rev. A* **1990**, *41*, 6763.

(20) Ohta, T.; Jasnow, D.; Kawasaki, K. *Phys. Rev. Lett*. **1982**, *49*, 1223.

(21) Lifshitz, M.; Slyozov, V. V. *J. Phys. Chem. Solids* **1961**, *19*, 35.

(22) Due to the A coating on the particles, the addition of these fillers alters the composition of the original A/B mixture. For example, in the case of 100 particles, the composition is shifted from the initial 50:50 critical mixture to a 53:47 slightly "off-critical" system. To test whether the particles or the effective off-criticality are responsible for the new morphology, we carried out simulations on a 53:47 AB blend without particles. These systems still display a bicontinuous structure. Thus, the disruption of the B network is directly due to the presence of the mobile particles, not the effective off-criticality of the mixture.

(23) Peng, G.; Ginzburg, V. V.; Qiu, F.; Jasnow, D.; Balazs, A. C. Unpublished.

(24) Gyure, M. F.; Harrington, S. T.; Strilka, R.; Stanley, H. E. *Phys. Rev. E* **1995**, *52*, 4632.

(25) Glotzer, S. C.; Gyure, M. F.; Sciortino, F.; Coniglio, A.; Stanley, H. E.; *Phys. Rev. E* **1994**, *49*, 247.

(26) Huse, D. A.; Henley, C. L. *Phys. Rev. Lett*. **1985**, *54*, 2708.

(27) Srolovitz, D. J.; Hassold, G. N. *Phys. Rev. B* **1987**, *35*, 6902.

(28) To emphasize that this slowing down is due to the presence of the particles and not the effective off-criticality of the mixture, we investigated the domain growth for a significantly off-critical binary mixture in the absence of particles. In particular, we focused on a 65:35 AB blend. We saw no significant deviation from the Lifshitz−Slyozov growth law over comparable times.

(29) The "cutting" by the particles is not an artifact of the Kawasaki exchange dynamics. Using a model that allows for a "smoother" motion of the particles, we observe the same structure.

(30) Note that the mobile particles not only drift in the shear flow, but also move randomly in the system. The latter motion "cuts" the long, striped domains that are formed under the imposed advection, and thus, decreases the effect of shear on the domains. Hence, the shear rate is effectively reduced in the presence of the moving particles. We include here a smooth dependence on particle density.

(31) Lauger, J.; Laubner, C.; Gronski, W. *Phys. Rev. Lett*. **1995**, *75*, 3576.

(32) Morkved, T. L.; Wiltzius, P.; Jaeger, H. M.; Grier, D. G.; Witten, T. A.; *Appl. Phys. Lett*. **1994**, *64*, 422.

(33) (a) Lin, B., et al. *J. Appl. Phys*. **1999**, *85*, 3180. (b) Zehner, R. W., et al. *Langmuir* **1998**, *14*, 241.

(34) Glotzer, S. C.; DiMarzio, E. A.; Muthukumar, M. *Phys. Rev. Lett*. **1995**, *74*, 2034.

(35) Oono, Y.; Bahiana, M. *Phys. Rev. Lett*. **1988**, *61*, 1109.

(36) Ohta, T.; Kawasaki, K. *Macrolmolecules* **1986**, *19*, 2621.

(37) Ginzburg, V. V.; Gibbons, C.; Peng, G.; Qiu, F.; Balazs, A. C. Modeling the Dynamic Behavior of Diblock Copolymer/Particle Composites. **Macromolecules**, submitted.